# RESEARCH Open Access



# Hydrodynamic parameter estimation of DARPA SUBOFF using dynamic pitch maneuver

Imran Mushtague<sup>1</sup>, Adil Loya<sup>1\*</sup>, Antash Najib<sup>1</sup>, Guogang Ren<sup>2</sup>, Jason Knight<sup>3</sup> and Abbas Hussain<sup>1</sup>

\*Correspondence: loya\_adil@yahoo.com

<sup>1</sup> Department of Mechanical Engineering, National University of Sciences and Technology, Islamabad, Pakistan <sup>2</sup> Department of Engineering and Technology, University of Hertfordshire, Hatfield, UK <sup>3</sup> School of Electrical and Mechanical Engineering, University of Portsmouth, Portsmouth, UK

## **Abstract**

The DARPA SUBOFF model is widely used for studying underwater vehicle performance, and many researchers have explored its behavior through experiments and simulations. The hydrodynamic flow over the underwater vehicle and its appendages during dynamic pitch maneuver is complex. Therefore, it necessitates conducting detailed flow analysis of boundary layer attachment and detachment while in a dynamic state. For this purpose, this study presents detailed insight on dynamic maneuver to capture the complete flow profile, flow field parameters, hydrodynamic effects, and vortex shedding behind stern appendages. In the present study, the transient maneuvering of the DARPA SUBOFF with respect to the lateral axis was carried out at multiple angles of attack from -30 to +30° while the sterns were deflected with an increment of 5° ranging from – 30 to 30°, and the data was recorded. This rotation of control surfaces actuated by 5° increment ranging from -30 to +30° provided 13 different simulations for actuation cases on which the dynamic pitch maneuver was carried out. However, literature shows most of these studies have focused on fixed control surfaces and only a few selected angles of attack (AoA). The hydrodynamic coefficients such as drag  $(C_d)$ , lift  $(C_l)$ , and and moment  $(C_m)$  are calculated for different pitching angles at a speed of 3.05 m/s. The results are first validated at zero AoA and then compared across various control surface angles. The coefficients showed consistent and systematic trends during the pitching motion, with C<sub>d</sub> ranging from 0.02 to 0.025,  $C_1$  from - 0.04 to 0.042, and  $C_m$  from - 0.015 to 0.012. This study provides more detailed insights into the dynamic behavior of underwater vehicles, which is important for improving their control and stability.

**Keywords:** Underwater vehicle, CFD simulations, Hydrodynamic coefficients, Control surfaces and star CCM+

### Introduction

The use of submarines and autonomous underwater vehicles (AUV) in the sea is growing in commercial, research, and military fields. An improvement in design efficiency and the establishment of innovative control approaches and methods are needed to make improvements in underwater technology. As the demand for these underwater systems increases, so does the need to improve their design, control, and



© The Author(s) 2025. **Open Access** This article is licensed under a Creative Commons Attribution 4.0 International License, which permits use, sharing, adaptation, distribution and reproduction in any medium or format, as long as you give appropriate credit to the original author(s) and the source, provide a link to the Creative Commons licence, and indicate if changes were made. The images or other third party material in this article are included in the article's Creative Commons licence, unless indicated otherwise in a credit line to the material. If material is not included in the article's Creative Commons licence and your intended use is not permitted by statutory regulation or exceeds the permitted use, you will need to obtain permission directly from the copyright holder. To view a copy of this licence, visit http://creativecommons.org/licenses/by/4.0/. The Creative Commons Public Domain Dedication waiver (http://creativecommons.org/publicdomain/zero/1.0/) applies to the data made available in this article, unless otherwise stated in a credit line to the data.

maneuverability. One important aspect in this regard is understanding how underwater vehicles respond to changes in fluid flow, especially during motion involving changes in orientation, such as pitching or turning.

A crucial factor affecting underwater vehicle performance is the Angle of Attack (AoA), the angle between the direction of motion and the oncoming fluid flow. Most earlier studies have investigated the effect of AoA on hydrodynamic forces and moments using static tests or simple motions, with control surfaces held fixed. For example, the widely studied DARPA SUBOFF model has served as a reference geometry in many experiments and simulations. Researchers like Liu and Huang [25] and Roddy [29] carried out wind tunnel and towing tank experiments to determine force and moment coefficients at selected AoAs. Similarly, Tonio et al. [32] used a semiempirical method (DATCOM) and computational fluid dynamics (CFD) to predict hydrodynamic stability variables at specific AoAs and fixed control surface angles.

While these efforts provide valuable data, they are often limited to a small number of conditions and do not fully capture the dynamic nature of real underwater motion. In actual operations, submarines do not move at constant orientation. They pitch, yaw, and roll continuously, and the interaction between AoA and control surface deflections becomes more complex. Despite this, very few studies have explored these combined effects under dynamic conditions.

Some progress has been made in this direction. For example, Cho et al. [9] used Planar Motion Mechanism (PMM) tests on submarines to estimate stability derivatives, while Hussain et al. [4] applied both PMM and rotating arm tests in CFD to extract hydrodynamic coefficients [4]. However, even these advanced approaches often rely on stepwise or static AoA values. The effect of continuously varying AoA (dynamic pitch motion) in combination with control surface actuation remains underexplored.

The flow pattern in deeper regions tends to be more complex and rotational, which is mathematically represented by a non-zero vorticity vector. This non-zero vorticity vector is generated due to the influences of the non-orthogonal component of the vorticity specially in three-dimensional flows [10]. Due to various flow interactions, the oceanic flow pattern is also highly complicated and rotates near submarines, ships, and huge remotely controlled vehicles, as well as near the free surface. Moreover, the hydrodynamic pressure field and wake field are estimated in detail by Peihao Li et al. [21] for DARPA SUBOFF, their study stated that the RANS model is capable of producing highly accurate estimation of pressure fields. In their study, they proposed that as the bottom distance decreases, the hydrodynamic pressure profile changes from "V" shape to "W"

Yu-Hsien Lin et al. investigated DARPA hydrodynamic coefficients using Large Eddy Simulation (LES) method. They conducted Planar Motion Mechanism (PMM) for analyzing different hydrodynamic parameters which were in a high level of agreement with that of experimental results [23].

Yichen Hao et al. used Deep Graph learning method for the fast prediction of wake field behind DARPA SUBOFF. They investigated an unstructured wake behind the propeller disk attached to DARPA SUBOFF with various geometrical parameters [14].

In another study, Wang et al. investigated breaking-vortex baffle addition to the horseshoe vortex around sail and fin; they also implemented the FW-H equation for analyzing sound pressure level during this breaking-vortex effect. They found that having a baffle around the sail reduces the noise level in the low frequency range [15].

During the vehicle's development phase, it is essential to figure out how well an underwater vehicle (UV) would maneuver. Newton's laws of dynamics are used to generate the equations of motion, which are then solved for predicting the movement of UV [1]. In the equations of motion, hydrodynamic coefficients (hydrodynamic derivatives) often describe the forces and moments impacting the vehicle. If hydrodynamic coefficients are determined precisely, they can be used in simulations to produce highly accurate outcomes. A possible method for testing a submersible vehicle's maneuverability is to use a physical self-propelled model in a towing tank for modeling trials. Another effective but complicated solution is the calculation of hydrodynamic coefficients using numerical techniques or analytical software like Maxsurf, Paramarine, or DATCOM, which are semi-empirical approaches. These techniques are particularly helpful during the design stages of a vehicle, providing a quick and simple option for design contingencies to these costly and time-consuming methodologies. Wu [22] thoroughly described and assessed the mobility of a UV sinking action by simulating a UV-forced self-propelled diving maneuver using several coarse hybrid grid and detachable region approaches. The increase of the boundary layers is virtually unrelated to the Reynolds number, according to Balaras [28], who investigated the impacts of the Reynolds number for SUBOFF. Wallmodeled Large Eddy Simulation (WMLES) can be used to reduce the need for very fine mesh resolution near the wall surface.

A submersible vehicle can be forcefully pulled downward when it encounters harsh wave conditions. Rapid sinking beyond safe depth limits may lead to severe damage, as seen in the KRI Nanggala-402 submarine tragedy. Gong et al. [12] investigated the strong internal solitary waves at the location of the Indonesian submarine wreck and highlighted how such oceanic features can contribute to such incidents [12]. It is necessary to investigate the hydrodynamic forces caused by waves to assess how they affect submarines. Moreover, Gong et al. investigated the presence of strong internal solitary waves near the location where the submarine sank. Their findings highlight how such underwater disturbances can pose significant risks to submerged vessels, and therefore directly support the relevance of studying hydrodynamic forces and wave effects on submarines.

The DARPAs underwater modeling, known as the DARPA SUBOFF underwater prototype, is the subject of most studies now being conducted for submarines [34]. Caplier et al. [6] evaluated sailing wakes in water depths and constrained water layouts under various Froude numbers, additionally, the research investigates the ship hull's resistance in depths and restricted water setups using a hydrodynamic balancing act. To study the velocity distribution surrounding the DARPA SUBOFF prototypes, Shin et al. [31] used the Reynolds Averaged Navier Stokes (RANS) approach. They also used the Volume of Fluid (VOF) approach to record the water-air interface. For various Froude numbers and various underwater levels, the hydrodynamic properties, including the resistance elements and the waves produced by the underwater prototype at the free surface, were estimated. Carrica [8] mathematically predicted the perpendicular zigzag mobility of a submersible using flexible system innovation, and practical findings confirmed the viability of the Computational Fluid Dynamics (CFD) simulation. Both experimental and

mathematical investigations on the hydrodynamics of an UV traveling at various velocities over inclined stream banks were given by Mitra et al. [26]. By contrasting the turbulence kinetic energy and Reynolds shearing stress portions, the experimental study was employed to validate the Reynolds-stress modeling system. The analysis revealed that even slight adjustments in testing ground slope dramatically increase drag. It was noted that drag forces were two times those of a level test platform at an inclination angle of 13°. Similar findings were seen when the UV was moving at a drift inclination.

With the advancement of computer technology, the performance and resolution of CFD simulations for hydrodynamic analysis of underwater vehicles and boats have significantly improved. However, the accuracy of these simulations remains dependent on the suitability of turbulence models and sensitivity to boundary conditions. Nevertheless, to set up the model as per the CFD approach, it is necessary to carry out a grid independence test, construct an independent assessment of a flow field, and evaluate the resolution as stated by Lin et al. [24]. Zhang [37] investigated the maneuverability of an UV by simulating a PMM by CFD employing the FLUENT software and collecting all associated hydrodynamic parameters. The findings demonstrated that an exact level of hydrodynamic parameters is required to construct an autonomous UV modeling system that serves as a starting point for an autonomous control system. CFD was used in a computational study to determine the effectiveness of the stern appendages of a highspeed submerged vehicle. When the cruciform was substituted for the X form design in a control effectiveness comparison with the cruciform, it was found that the effectiveness improved by 40% [18]. To allow for dynamic control surface deflection during specific maneuvers, Pankajakshan et al. [15] used a deformable mesh [27]. In a multibody interaction investigation conducted by Dreyer and Boger, a control algorithm was used to guide a "free running" submarine [11]. Instead of using dynamic control surface deflections in their simulation, they used external forces. Due to the adaptability of UVs in supporting a variety of undersea missions, such as oceanographic studies, offshore gas extraction, and military missions, the study and development of submersibles and AUVs has resulted in an increase in demand in the oceanic engineering society as per Cardenas et al. [7]. When performing movements like steady turning, depth changes, submarines and AUVs must maintain their stability. Therefore, when designing vehicles, it is necessary to develop a system for estimating how submarines and AUVs will behave during such operations. It is common practice to compute movement simulations and motion control design using mathematical models of submarines and AUVs. A nonlinear mathematical representation with a full set of hydrodynamic coefficients is necessary, as also modeled by Heberley and Hui et al. [16] and Hui, Jinyun et al. [17]. Their mathematical model can accurately reproduce several types of movements, such as straight lines, turning in circles, or zigzag, if desired.

Researchers have recently focused a lot of their attention on the maneuverability and hydrodynamic performance of submarines and other UVs, as stated by several researchers like Kim, Kim et al. [19], Shahinfar, Bozorg et al. [30], and Cho, Seok et al. [9]. The most well-known of these are the SUBOFF submarines. DARPA suggested the SUBOFF project in the 1990s with the intention of using CFD technology to help in the design of submarines in the future [29]. Numerous researchers tested SUBOFF extensively and verified it using CFD, and they also provided plenty of useful information. The surface

pressure of the DTRC Model 5471 model's hull was determined by Liu and Huang [25] in a wind tunnel at various inflow speeds. The test results not only offer solid data support for the SUBOFF model's hydrodynamic analysis, but they also serve as a crucial foundation for confirming the accuracy of numerical calculations in the years to come. In the Virginia Tech Stability wind tunnel, Whitfield [36] carried out the steady and unsteady force and moment experiments of SUBOFF. Various body designs for the SUBOFF model were examined in two distinct test sections. They tested four different designs: (a) bare body hull, (b) body with sail, (c) body with stern appendages, and (d) body with sail and stern appendages were the body designs for both the steady and unsteady studies. By utilizing Large Eddy Simulation (LES), Alin, Fureby et al. [2] investigated the flow characteristics around the SUBOFF bare hull and fully appended hull designs. The forces and moments on the SUBOFF in a steady turn were examined using numerical simulations by Leong, Ranmuthugala et al. [20], Toxopeus, Atsavapranee et al. [33], and Cao, Zhu et al. [5]. Tonio et al. [32] calculated the force and moment coefficients for an axisymmetric streamlined body DARPA SUBOFF submarine model (DTRC 5470) at various AoA using the semi-empirical approach (DATCOM). They matched the outcomes with the experimental data found in DTRC literatures, as described in Liu and Huang [25] and Roddy [29]. One of the key factors to consider when developing unmanned submerged vehicles is maneuverability.

It is pertinent to mention that the research conducted using Experimental Fluid Dynamics (EFD) is a tedious method to find different forces and moments. It is highlighted in the Angela Susan Tonio et al. [32] paper that experimentally the data for forces and moments was gathered using resistance test in towing tank facility with a varying speed from 3 to 9 m/s. Next, they even conducted flow profile test using Anechoic Flow Facility using wind tunnel to measure pressure, wall shear stress and velocity profile. Finally, they also used the Oblique test, i.e., PMM to find the stability variables of the DARPA SUBOFF. These tests require big facilities and tests can only be conducted on particular angle of interest. Angela Susan Tonio et al. [32] also used numerical solver, i.e., DATCOM for hydrodynamic stability analysis. DATCOM requires a data input file regarding the geometric aspect of DARPA SUBOFF, then it calculates the hydrodynamic stability variables using several equations of motions and vortex lattice method. Nevertheless, the third method used by Angela Susan Tonio et al. [32] was CFD in which they used DARPA SUBOFF at specific AoA to determine the stability and maneuvering parameters.

Moreover, the second research method, which is of great importance when finding the stability parameters of the AUV, is the PMM test. This test is performed by Yong Jae Cho et al. [9] on BB2 submarine. This test provides details with regard to the coefficients of hydrodynamic stability and control derivatives. They used STAR CCM+ and SNU-FOAM for collecting their PMM results.

Out of the above three mentioned techniques, nowadays researchers are using control and observer-based techniques to identify the hydrodynamic stability and control parameters using system identification. Joonyoung Kim et al. [19] used a sliding mode observer to identify the stability parameters and an Extended Kalman Filter for depicting the stability variables using a non-linear stochastic technique for plant perturbation and sensor noise evaluation.

It is important to mention here that Hussain et al. [4] used CFD technique with two different methods to identify the stability and control derivatives of the DARPA SUB-OFF using PMM and Rotating Arm Test. By keeping in mind these several techniques of research, in current research CFD technique was adapted; however, it was ensured that data is gathered with utmost accuracy and precision, which was only possible using dynamic transient rotation.

### **Novel aspect**

While several experimental and numerical studies have investigated the hydrodynamic behavior of the DARPA SUBOFF model, most existing works focus on limited angles of attack (AoA) ranges or specific control surface deflections under static conditions. Moreover, many rely on time-consuming mesh reconstruction for each configuration or do not fully explore dynamic simulations over a continuous range of orientations.

The current study addresses this gap by conducting dynamic rotation simulations of the DARPA SUBOFF model across a wide AoA range (- 30° to + 30°) with deflection of a control surfaces setting. This approach allows the collection of a large and continuous dataset without requiring reconfiguration of the mesh or boundary conditions for each test case. The results are compared with available experimental data to validate the accuracy.

The novelty of this research lies in using dynamic AoA rotation within a CFD environment (STAR CCM+) to extract a full set of forces and moments and their coefficients in one simulation sequence an—approach not widely adopted in previous studies. This makes the findings highly suitable for control system design and performance prediction of autonomous underwater vehicles.

It is pertinent to mention that during the continuous discrete simulation, the generation of the wake around the control surfaces and behind the snorkel provides detailed insight into the vortex variation during the continuous change of angle of attack (AoA), which produces streamlines that demonstrate the horseshoe effect and circulations. This continuous approach opens the physical effect of the boundary layer detachment behind and underneath the control surfaces and predicts various types of vortices.

# Methods

In addition to above, the current study examines possible application of a numerical approach (Star CCM+) to estimate the force and moment parameters and their coefficients for an axisymmetric streamlined body DARPA SUBOFF submersible model (fully appended and hull form) with deflection of control surfaces from  $-30^{\circ}$  to  $+30^{\circ}$ with steps of 5°; however, the body was rotated dynamically from  $-30^{\circ}$  to  $+30^{\circ}$  AoAs with static control surface. During dynamic rotation, the results have been collected at every step from -30 to  $+30^{\circ}$  AoAs. This method of rotating the body dynamically through a continuous range of angles of attack with deflection of the control surfaces reduces the need for multiple simulation setups, mesh reconstructions, and reinitialization of physical parameters, an approach that has not yet been widely explored in previous studies. Moreover, outcomes contrasted with experimental findings from DTRC publications, as stated in Liu and Huang [25] and Roddy [29], provide a detailed comparison, nevertheless, the data available from their research provide certain or specific

data for some specific AoAs with variable control surface position. This study aims to generate a dense dataset of hydrodynamic forces and moments over a wide range of angles of attack, which is valuable for developing and validating control algorithms for underwater vehicles. While the simulations are bound by selected modeling parameters, the comprehensive nature of the data enhances its usefulness for system identification and maneuverability prediction. Moreover, detailed insight is also provided regarding the formation of horseshoe vortex underneath appendage and its effect on the complete body is also discussed. The Resistance Test and Oblique Test accuracies of the CFD results are validated with experimental results.

# **Governing equations**

The equations used for solving fluid flow and analyzing flow field parameters were of continuity, momentum equation, and  $k-\omega$  SST turbulence model equations. The following equations are provided below from Eqs. (1) to (5).

The derivation of conservation of mass is dependent upon the principle of mass balance within the fluid element. Equation (1) shows the law of mass conservation (Sun and Zhang 2020).

$$\frac{\partial \rho}{\partial t} + \nabla \times (\rho \times v) = 0 \tag{1}$$

In Eq. (1), the first term is a material property, while the time change and the additional change in volume of moving fluid are also included. The momentum equations in the x, y, and z coordinates, respectively, are expressed by Eq. (2), (3), and (4), given below [35].

$$\frac{\partial(\rho \mathbf{u})}{\partial \mathbf{t}} + \nabla \times (\rho \mathbf{u} \mathbf{V}) = -\frac{\partial \mathbf{p}}{\partial \mathbf{x}} + \frac{\partial \tau_{xx}}{\partial \mathbf{x}} + \frac{\partial \tau_{xy}}{\partial \mathbf{y}} + \frac{\partial \tau_{xz}}{\partial \mathbf{z}} + \rho \mathbf{f}_x \tag{2}$$

$$\frac{\partial(\rho \mathbf{v})}{\partial \mathbf{t}} + \nabla \times (\rho \mathbf{v} \mathbf{V}) = -\frac{\partial \mathbf{p}}{\partial \mathbf{y}} + \frac{\partial \tau_{yx}}{\partial \mathbf{x}} + \frac{\partial \tau_{yy}}{\partial \mathbf{y}} + \frac{\partial \tau_{yz}}{\partial \mathbf{z}} + \rho \mathbf{f}_{\mathbf{y}}$$
(3)

$$\frac{\partial(\rho w)}{\partial t} + \nabla \times (\rho wV) = -\frac{\partial p}{\partial z} + \frac{\partial \tau_{xz}}{\partial x} + \frac{\partial \tau_{yz}}{\partial y} + \frac{\partial \tau_{zz}}{\partial z} + \rho f_z \tag{4}$$

The energy equations used were derived by Navier-Stokes, which is based upon the first law of thermodynamics. The derivation for conservation of energy on a finite fluid element consists of one equation. Using this equation, we can apply viscous phenomena to predict true stress around the body and its factors of wall shearing. This induces skin friction on the boundary layers as the flow is propagated. This viscous effect is introduced using  $\tau$  terms involved in Eq. (5) as shown below:

$$\begin{split} & \left[ \rho \left( e + \frac{V^2}{2} \right) \right] + \nabla \times \left[ \rho \left( e + \frac{V^2}{2} \right) V \right] = \rho \dot{q} + \frac{\partial}{\partial x} \left( k \frac{\partial T}{\partial x} \right) + \frac{\partial}{\partial y} \left( k \frac{\partial T}{\partial y} \right) + \frac{\partial}{\partial z} \left( k \frac{\partial T}{\partial z} \right) - \frac{\partial \left( up \right)}{\partial x} - \frac{\partial \left( vp \right)}{\partial y} - \frac{\partial \left( wp \right)}{\partial z} \right. \\ & + \frac{\partial \left( u\tau_{xx} \right)}{\partial x} + \frac{\partial \left( u\tau_{xx} \right)}{\partial y} + \frac{\partial \left( v\tau_{xy} \right)}{\partial z} + \frac{\partial \left( v\tau_{yy} \right)}{\partial y} + \frac{\partial \left( v\tau_{yz} \right)}{\partial z} + \frac{\partial \left( w\tau_{xz} \right)}{\partial z} + \frac{\partial \left( w\tau_{yz} \right)}{\partial z} + \frac{\partial \left( w\tau_{zz} \right)}{\partial z} + \rho f \times V \end{split}$$

Multiple approaches have been used for determining the coefficients of fundamental hydrodynamic parameters. The three essential variables and their coefficients must be calculated for longitudinal hydrodynamic control to evaluate the control performance of the DARPA SUBOFF body. These parameters are drag force and drag coefficient ( $C_D$ ), lift force and lift coefficient ( $C_L$ ), and pitching moment coefficient ( $C_m$ )

The dimensionless coefficient of drag is known as  $C_D$ . This force coefficient calculates the drag forces acting on the body's flow. This is a crucial element in figuring out how smoothly the body will move as it moves in the opposite direction of the fluid flow. Equation (6) gives a description of the drag force coefficient.

$$C_D = \frac{F_D}{\frac{1}{2}\rho v^2 A} \tag{6}$$

Whereas

 $C_D = Drag$  force coefficient,  $F_D = Drag$  Force,  $\rho = Density$  of liquid  $\nu = Velocity$  of fluid,

A =Reference area of the body

The lift forces impacting on the body are measured using a force coefficient called coefficient of lift  $C_L$ , which has no dimensions and is oriented in the direction of the Y axis. This force assists the body in moving upward, acting in the opposite direction to the body's weight. Equation (7) displays the formula of lift force coefficient.

$$C_L = \frac{F_L}{\frac{1}{2}\rho v^2 A} \tag{7}$$

Where, C<sub>L</sub> Lift force coefficient, F<sub>L</sub> Lift Force

The standard abbreviation for the pitching moment coefficient is  $C_m$ . This moment coefficient describes the body's pitching moment with respect to the position of its center of gravity (COG). For evaluating the under-vehicle dynamic stability with respect to its COG location,  $C_M$  is an essential parameter. The formula of pitching moment coefficient is given using Eq. (8).

$$C_m = \frac{M}{\frac{1}{2}\rho v^2 AL} \tag{8}$$

Whereas

 $C_m$  = pitching moment coefficient and M = pitching moment.

# Workflow and geometry

For a DARPA SUBOFF project in 1989, Groves et al. [13] developed an axisymmetric SUBOFF with symmetrical appendages at the stern. This designed SUBOFF has an overall length of 4.3560 m. Due to the confidential nature of the investigations, submarine hull forms and accompanying experimental data are often not available. However, its geometry is freely accessible, and a wide range of experimental results are available for verification with CFD results. In this study, we have adopted the dynamic pitch maneuver of DARPA SUBOFF at multiple AoAs with deflection of control

surfaces, i.e., stern appendages. Different hydrodynamic parameters have been calculated and validated with experimental findings.

The dynamic transformation of the submarine is realized by changing its angles of attack, which was set up as initial boundary condition. Every second, the body tilts up to  $3^{\circ}$ . Therefore, for up to 20 s, the whole body is rotated automatically from  $-30^{\circ}$  upward to  $+30^{\circ}$  downward. The submarine is rotated using a rotating mesh, which adapts automatically on the static mesh.

The trials were conducted on DARPA SUBOFF model with different forms such as fully appended hull, the hull with a sail, the hull with a ring wing, and the hull with no appendages as stated by Liu and Huang [25]. The fully appended form of the DARPA SUBOFF's with geometric parameters is provided in Fig. 1.

# Computational domain and boundary conditions

Initially the three-dimensional body displayed in Fig. 1 was designed in SolidWorks by utilizing the dimensions Listed in the same figure. This SolidWorks 3D model was exported in IGES format and imported into Siemens STAR-CCM+ to create the simulation setup. The domain configuration carried out before running simulations is provided in Fig. 2. In Fig. 2, there are two domains setup; one is static region shown in Fig. 2a and the second one is rotating region shown in Fig. 2b. The cylinder was assigned a rotational motion, while the block remained fixed as a stationary component.

Boundary conditions are essential to CFD as they define the flow direction of stream parameters like energy, mass, and momentum between other variables. Boundary conditions have been defined by developing a computational domain and using a function split by patch to denote the block's inlet, outlet, and symmetry conditions. The inlet was regarded as the velocity inlet. Because of the static pressure conditions at the outflow boundary, the exit was assumed as a pressure outlet. At the sides, top, and bottom of the whole domain, symmetry conditions have been considered. SUBOFF body was regarded as a no-slip boundary condition. Before starting the simulation, the following boundary conditions have been identified. Table 1 shows the parameters set up before the simulation.

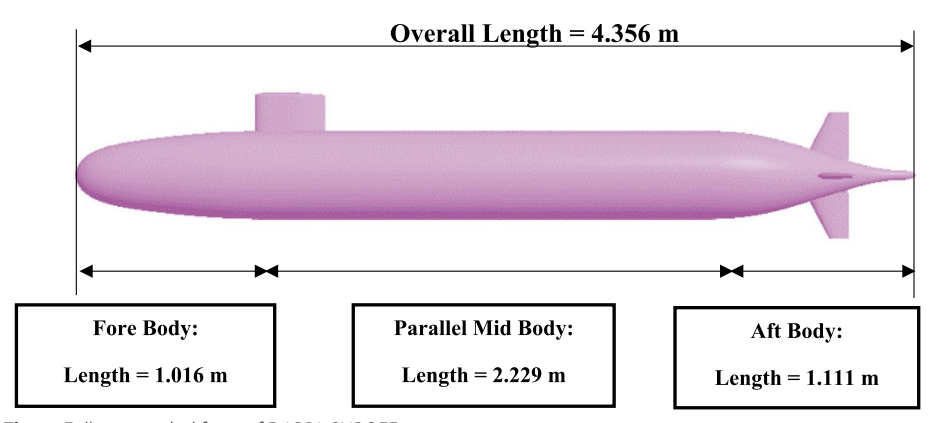


Fig. 1 Fully appended form of DARPA SUBOFF

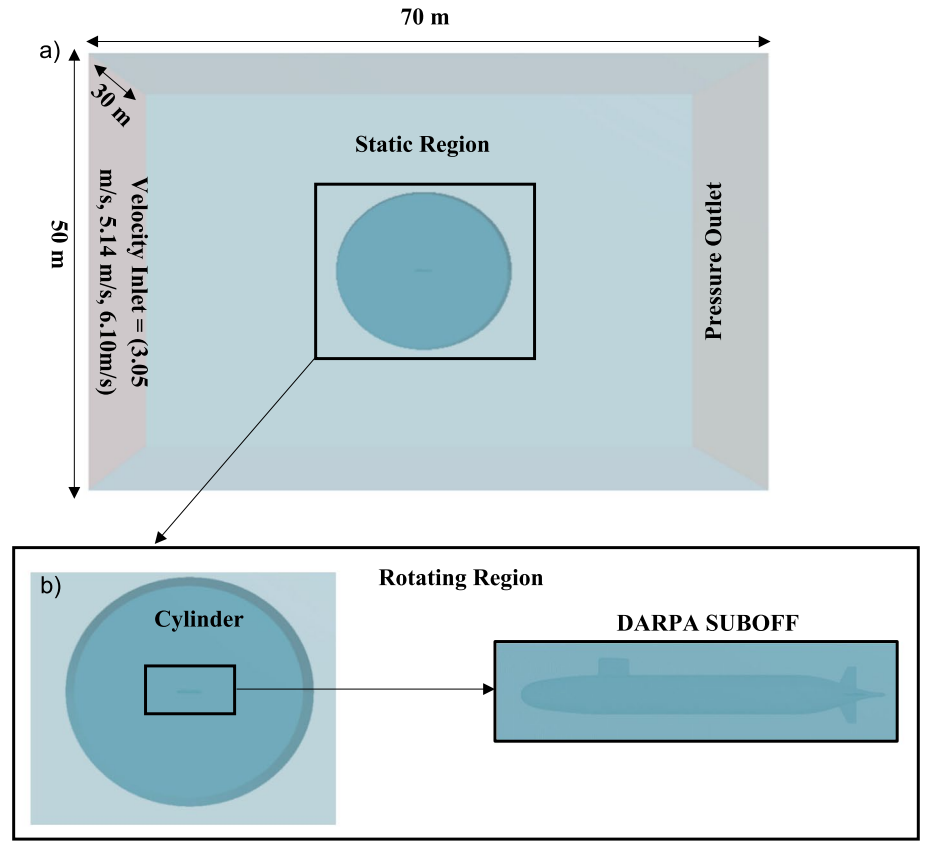


Fig. 2 Computational domains: a Upper image static domain and b Bottom rotating domain

Table 1 Boundary conditions

Reference parameters	Reference values
Inlet velocities	3.05, 5.14, 6.10 m/s
Pressure	101325 Pa
Density	997.561 kg/m <sup>3</sup>
Dynamic viscosity	0.00088871 Pa sec
Rotational rate	3°/s

The rotation rate of the rotating domain was set at 3°/s. Figure 2 displays a magnified image of the complete computational domain and the boundary conditions that were considered. Here it is pertinent to mention that the control domain in which the desired body was placed for carrying out analysis for flow field parameters was rotated about the *z*-axis, as the *z*-axis is the lateral axis about which the pitch moment is produced.

# **Modeling physics**

The basic parameters of the simulation (such as pressure and velocity) are specified by physics models, together with the mathematical procedure that is used to generate the solution. A suitable set of models must be combined to fully define a physics continuum. A physics continuum (such as air and water) contains the models used to depict the flow of the selected fluid. In the present study, water (a liquid) is the chosen fluid flow because of its turbulent nature. After meshing, physical conditions were set up for calculating hydrodynamic parameters. For this, RANS was employed in conjunction with two-equation model, i.e., SST  $k-\omega$ . SST  $k-\omega$  was selected since it is a hybrid model that includes both  $k-\omega$  and  $k-\varepsilon$ . The flow closest to the wall is most effectively expressed by  $k-\omega$ , while the flow farthest from the wall is better represented by  $k-\varepsilon$ . This model ensures the shear stress and wake depiction is efficaciously produced as the dynamic pitch maneuver takes place. The all Y+ treatment was necessary as the interest was not only limited to boundary layers but also towards the wake behind the vehicle. The fluid of consideration is water; as the object is an underwater vehicle, therefore, the density was kept constant, and an unsteady time domain was selected for transient simulation.

The dynamic simulation is performed at 3 different velocities, i.e., 3.05 m/s, 5.14 m/s, and 6.10 m/s. These velocities were set one by one in the simulation setup. In addition to this, the rotational rate was also set in the simulation setup, i.e., every 1 s the body is transformed at 3° to achieve dynamic pitch maneuver.

# Mesh generation

One of the most crucial factors that must be considered to achieve simulation validity is outstanding mesh creation. It has a direct impact on time, convergence, and output correctness. Part base meshing and region base meshing are the two forms of meshing. Part base meshing is employed in this study by using the automated mesh button in Star CCM+. The meshers used in this study are polyhedral and trimmer. The polyhedral is applied to the rotating domain, which includes the cylinder and body, while the trimmer is used on the block, which is a motionless part in the study. The polyhedral mesh is good for complex geometries and provides more accurate results as compared to other meshers. However, the trimmer cells alignment and cell quality are very good, and it also provides better results. This scheme is better for solving boundary layers and accurate prediction of flow near walls. The volume mesh was created using a trimmed cell mesher since it was particularly effective at converging the solution. Consequently, hexahedral grid cells are used to divide up the entire region being meshed.

Furthermore, custom controls were applied to the sail and control surfaces of the body to further improve the mesh as shown in Fig. 3. With the Help of meshing ideas, different values for the base size, surface size, thickness of the prism layer, number of prism layers, surface curvature, and other variables have been attempted to produce the refined mesh of the complete domain. The most refined mesh generated had 29,021 grid elements in the static region, and the rotating mesh grid had 938,388 elements. A boundary layer mesh with a first cell Height of 0.00346 m was applied, based on Y<sup>+</sup> calculations for accurate near-wall resolution using the SST k-ω turbulence model. A total of 7 prism layers were used to capture the full boundary layer profile along the submersible surface. The exact nature of the flow close to the wall is improved by this layer of cells. Figure 3 displays a representation of the prism layer close to the surface of the body in terms of mesh generation. Moreover, the wake region around the appendages is also displayed in Fig. 3.

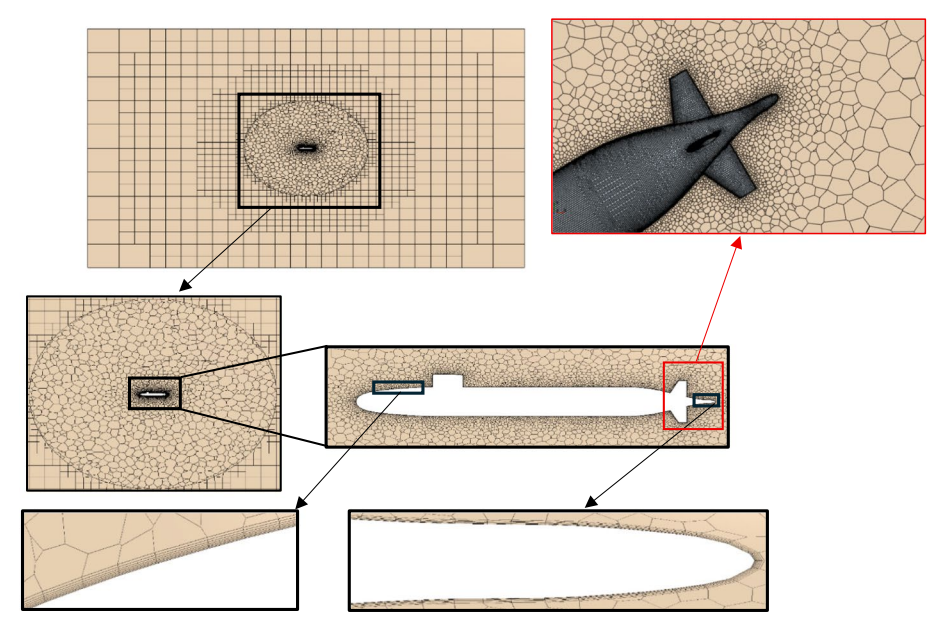


**Fig. 3** Mesh depiction of computational domain and wake region behind the appendages is shown with red outline

# Mesh independence study

To determine the effect of cells on the simulation outcomes, the drag force and its coefficient were computed for various cell counts during the process of convergence analysis. The drag force and its coefficient were identified for various base sizes for the mesh independence research. Mesh density rises as base size decreases and vice versa, as shown in Table 2.

The simulation results for the drag force in the case of the static position of DARPA SUBOFF model and its coefficient were convergent at 450,000 cells, and this also provided fine meshing, which is also shown in the convergence analysis in Fig. 4. Consequently, to perform further simulations, a base size of 0.1 m was chosen.

However, the grid independence and time independence study with respect to AoAs has been carried out in the case of a dynamic pitch maneuver at multiple base sizes and time steps as shown in Fig. 5a–f, respectively. Figure 5a–c shows the dynamic grid independence study with respect to angles of attack (AoA) of drag, lift, and pitching moment at multiple base sizes. On the other hand, Fig. 5d–f shows the time independence graphs with respect to angles of attack (AoA) in the light of dynamic

**Table 2** Base size with different mesh quality used for convergence analysis

	, ,	,
Base size (M)	No. of cells	Grid density
0.1	450082	Very fine
0.13	288952	Fine
0.15	234096	Slightly medium
0.27225	102831	Medium
0.5445	54790	Slightly coarse
1.089	40539	Medium coarse
2.178	36171	Coarse

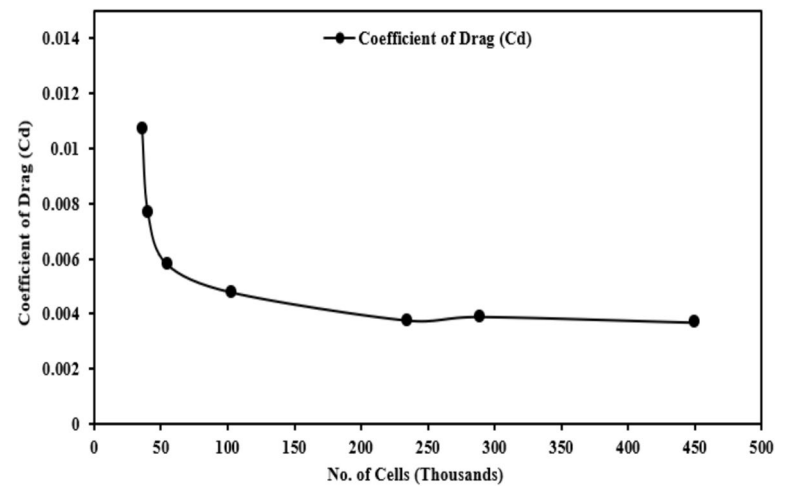
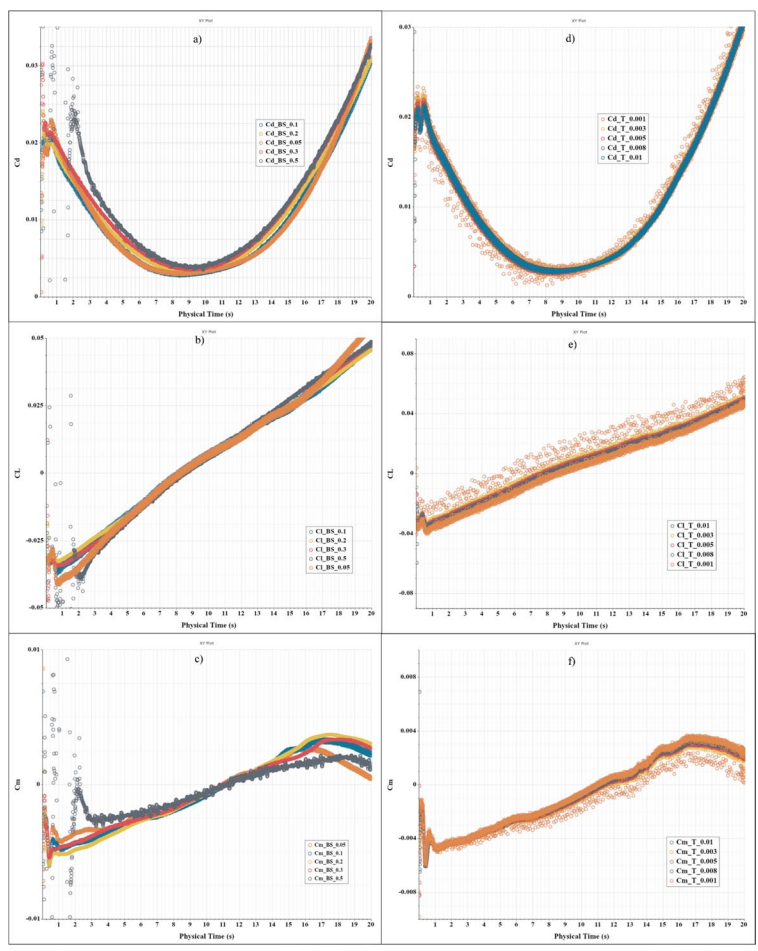


Fig. 4 Mesh convergence study of coefficient of drag (Cd)



**Fig. 5** Mesh convergence study: **a** coefficient of drag (Cd), **b** lift coefficient (Cl), **c** pitching moment coefficient (Cm). Time independent study, **d** Drag coefficient (Cd), **e** Lift coefficient, **f** pitching moment coefficient (Cm)

pitch maneuver at multiple time steps. The graphs given show that the results have converged at multiple base sizes and time steps with respect to the change in AoA.

# Mesh quality

The residual output that is acquired at the end of each run is used to illustrate the correctness of the expected results and the outcome of the properties of the flow fields that are investigated during various dynamic simulations at numerous AoAs. It is important to note that, to get higher approximations of results, the residuals of flow, continuity, momentum, and other turbulence factors should be treated below the  $10^{-3}$  level. As a result, Fig. 6 shows the residual results following a successful run of a particular simulation. The level of convergence of the current research is represented by the residuals in Fig. 6.

In addition to validation and convergence, the quality of the cells developed during mesh formation was confirmed by checking the factor of skewness angle and the cell quality of the entire computational domain. Mesh generation and quality are known to be dependent on the factors mentioned above. The skewness angle and cell quality of the entire body and computational domain are shown in Figs. 7a, b and 8a, b, correspondingly.

Furthermore, in every set of dynamic simulation, before going on to the next step, the model is rotated from one AoA of study to another AoA, making sure that it fulfills the convergence of the previous one. It is worth mentioning over here that the frequency of skewness factor for the current model and the entire domain was found to be way within the Limit of 90° of skewness angle [3], which can be seen from Fig. 8a, b respectively.

In addition to the skewness, mesh cell quality was also determined for knowing the accuracy of the mesh generation. It was found that the frequency of the cell quality for the generated mesh was well within the Limits of 0.9 [3].

# Solution stability

It is well stated that before performing simulation, finding Courant number is necessary for knowing stability and accurate temporal discretization. Therefore, for this purpose, the Courant number was calculated beforehand to predict stable results during implicit unsteady run. Moreover, this is the reason the simulations conducted within this study at different time-step sizes produced highly stable non-diverging results as shown in Fig. 5d–f, thereby showing the efficacy of the produced outcomes. Courant number was calculated using Eq. (9).

$$Co = \frac{u \cdot \Delta t}{\Delta x} = \frac{3 \cdot 0.01}{0.1} = 0.3$$
 (9)

Where u is the flow velocity,  $\Delta t$  is the timestep size,  $\Delta x$  is the grid size and Co is the Courant number.

The above time-steps were chosen, keeping in mind the grid size and flow velocity in concern. This produced stable results on different time-step gradients as also depicted from Fig. 5d–f.

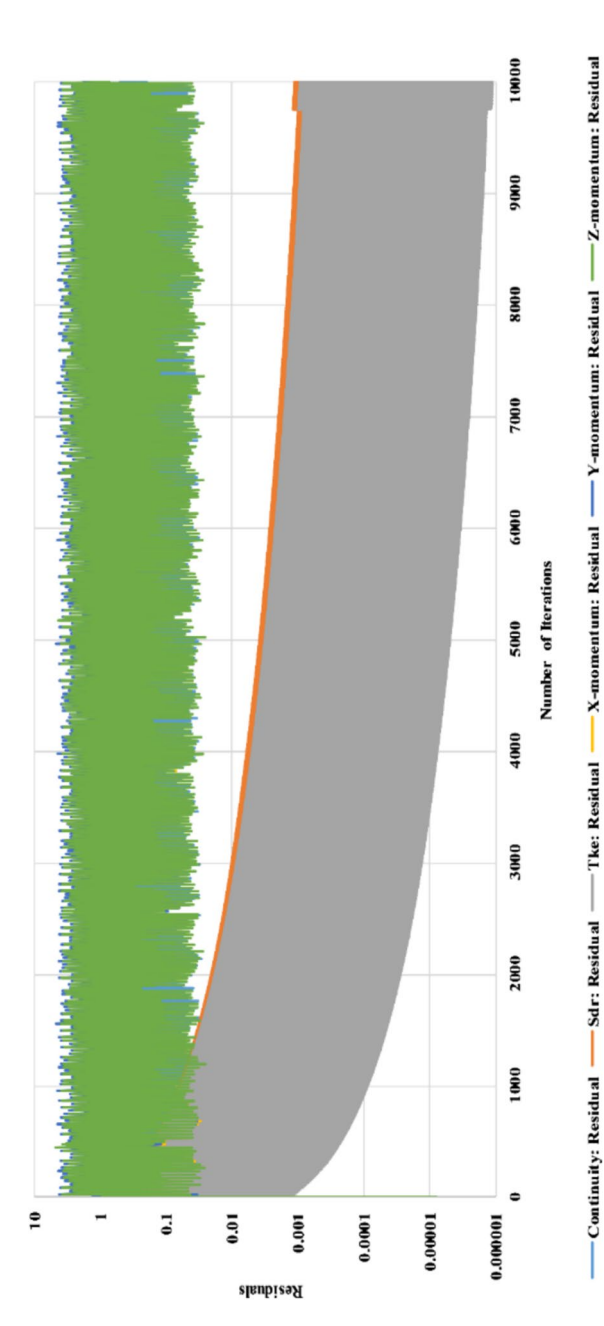


**Fig. 6** Residuals of simulation performed at  $-10^\circ$  control surface deflection angle at various angles of attack, i.e., from  $-30^\circ$  to  $30^\circ$ 

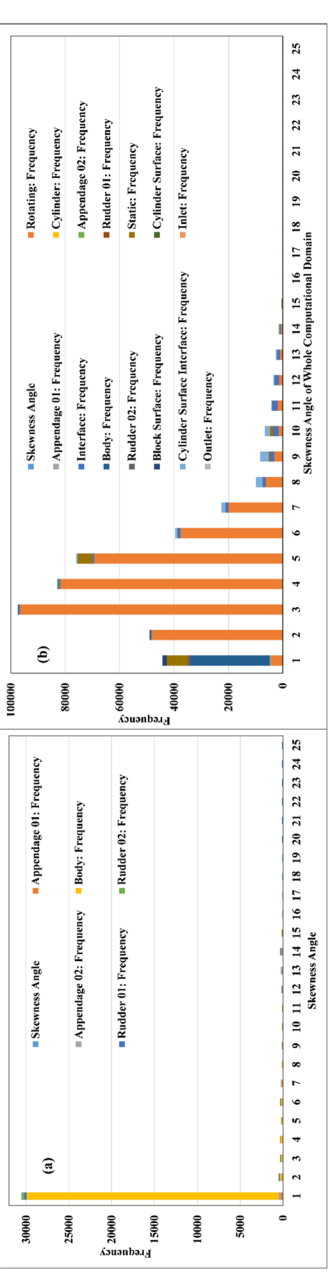


Fig. 7 a Skewness angle of the model. b Skewness angle of whole computational domain



Fig. 8 a Cell quality of the model. b Cell quality of whole computational domain

Table 3 shows that the courant number is below 0.3, showing good temporal resolution and demonstrating accurate resolution of the vortex shedding and generation of vortices. Moreover, from simulation, the courant number is found to be within the desired Limit of 0 to 1. This depicts that the boundary conditions, initial setup with respect to implicit unsteady condition, and consideration of courant number have evolved to produce and depict highly converged results. This is also shown using Fig. 9.

To put it in a nutshell, the selection of courant number is important to compute the results with optimum time and grid size to attain converging results with higher computational efficiency. Therefore, for all cases of simulations, Courant number was calculated around 0.305, which is the first value in Table 3, and accordingly, the relevant time-step size and grid size were set according to this value.

# **Results and discussion**

# Drag resistance validation at zero pitch angle

The EFD data was collected from study of R. Roddy [29] and H. L. Liu and T. T. Huang [25] for validating the resistance values provided in Table 4. Drag as well as  $C_D$  of the fully appended hull form was computed at 3.05 m/s. It is contrasted with the outcomes of the experiment. The drag of the bare hull form was estimated at 3.04 m/s using an identical methodology. The results are presented in Table 4.

As can be seen in Table 4, there is a very good correlation between results for the bare hull, whereas the difference between the results for the appended hull indicates that the error is under 7%. After this confirmation, the resistance of the DARPA SUBOFF's fully appended hull form and bare hull form was calculated at various speeds. Tables 5 and 6 list the experimental readings of resistance and  $C_D$  for the DARPA SUBOFF of fully appended hull form and bare hull form as well as the variance in the CFD results for various flow speeds. Figure 10a, b depicts the total resistance and  $C_D$  plot of the DARPA SUBOFF's fully appended and bare hull form, correspondingly.

The findings demonstrate that drag rises in a quadratic way as speed goes up. The findings of the CFD were contrasted with those from experiments, and it was determined that the error rate was less than 8% for all simulations. The Cd is noted to decrease slightly at higher flow speeds for both experimental and CFD simulations. This is regarded as a Reynolds number effect and is expected to continue to the full scale. Figures 11a, b, accordingly, depict the velocity depiction of fully appended and bare hull forms of DARPA SUBOFF at 3.05 m/s.

The streamlines depiction of DARPA SUBOFF of fully appended hull form at 3.05 m/s is shown in Fig. 12 with zoomed-in sections of the sail and hull section.

Due to the fluid's viscosity, whenever it moves over any surface, the molecules at the surface are at rest. The fluid that is located outside of the boundary layer is not slowed down. In the boundary layer, the fluid's velocity increases until it reaches the free stream velocity. Choosing the value of wall y+ is one of the most important stages in CFD simulations to gain accurate predictions. The size of the mesh and growth rate of the body are changed to keep wall y+ values within an acceptable range. Figure 13a, b shows the depiction of wall y+ value of the body. In the present research, the value of wall y+ is in the range of 0 to 30, as can be seen in Fig. 13. Ideally, when using all y+ turbulence models, the y+ should be below 15. Over most of the body, the y+ is below 15, but there are

Table 3 Courant number study

$\Delta t$ (s)	u <b>(m/s)</b>	$\Delta x$ (m)	Со
0.01	3.05	0.1	0.305
0.008	3.05	0.1	0.244
0.005	3.05	0.1	0.1525
0.003	3.05	0.1	0.0915
0.001	3.05	0.1	0.0305

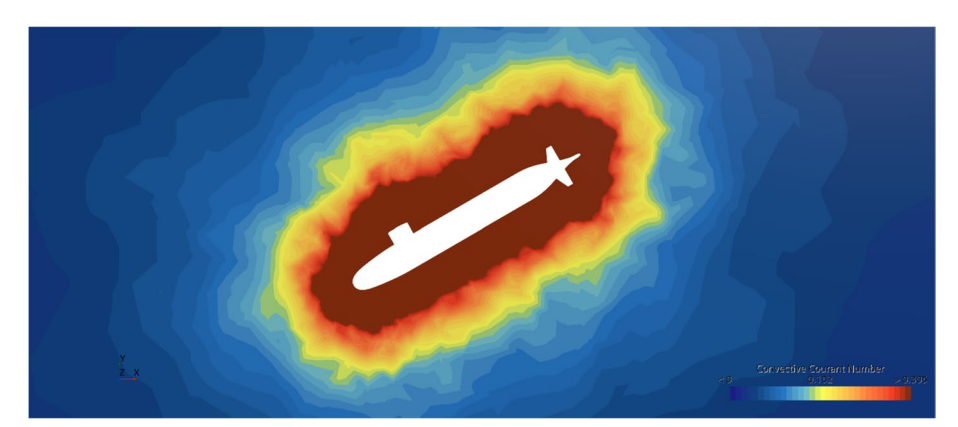


Fig. 9 Depiction of courant number attained from simulation

 Table 4
 EFD and CFD outcomes for fully appended hull form and bare hull form

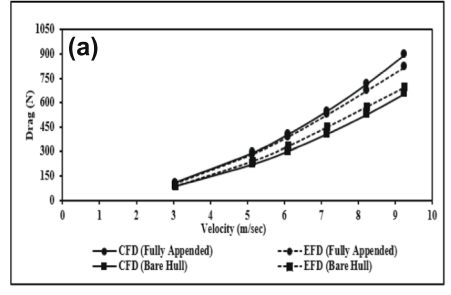
Model	CFD	EFD	Error (%)
Drag (N) (fully appended hull form)	108.779	102.3	6.333
Drag (N) (bare hull form)	86.403	87.4	- 1.139
Cd (fully appended hull form)	0.003693	0.003473	6.336
Cd (bare hull form)	0.003109	0.003145	- 1.133

Table 5 CFD and EFD resistance values for fully appended hull form and bare hull form of DARPA SUBOFF at various velocities

Velocity (m/s)	Resistance (N)				Error (%)	
	EFD (bare hull form)	EFD (fully appended hull form)	CFD (bare hull form)	CFD (fully appended hull form)	CFD (bare hull form)	CFD (fully appended hull form)
3.05	87.4	102.3	86.403	108.779	<b>–</b> 1.139	6.333
5.14	242.2	283.8	221.664	291.659	<b>-</b> 8.478	2.769
6.10	332.9	389.2	302.416	403.972	<b>-</b> 9.156	3.795
7.16	451.5	526.6	407.474	548.575	<b>-</b> 9.751	4.172
8.23	576.9	675.6	527.591	716.262	<b>-</b> 8.547	6.018
9.25	697.0	821.1	655.808	896.260	<b>-</b> 5.909	9.153

Velocity (m/s)	Cd				Error (%)	
	EFD (bare hull form)	EFD (fully appended hull form)	CFD (bare hull form)	CFD (fully appended hull form)	CFD (bare hull form)	CFD (fully appended hull form)
3.05	0.00314	0.00347	0.00310	0.00369	- 0.987	6.431
5.14	0.00306	0.00338	0.00280	0.00348	<b>-</b> 8.215	3.154
6.10	0.00300	0.0033	0.00272	0.00342	<b>-</b> 9.013	3.903
7.16	0.00294	0.00324	0.00266	0.00337	<b>-</b> 9.5	4.307
8.23	0.00285	0.00315	0.00260	0.00333	<b>-</b> 8.508	6.026
9.25	0.00272	0.00309	0.00256	0.00330	- 5 669	7 064

Table 6 CFD and EFD Cd values for fully appended hull form and bare hull form of DARPA SUBOFF



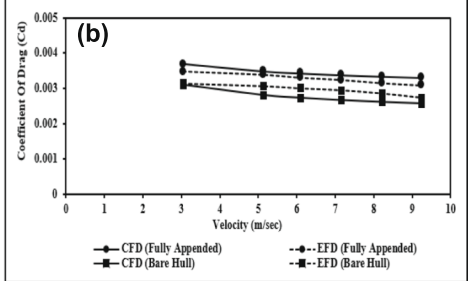


**Fig. 10** Graphs of fully appended hull form and bare hull form of DARPA SUBOFF. **a** The total resistance and b  $C_D$  plot

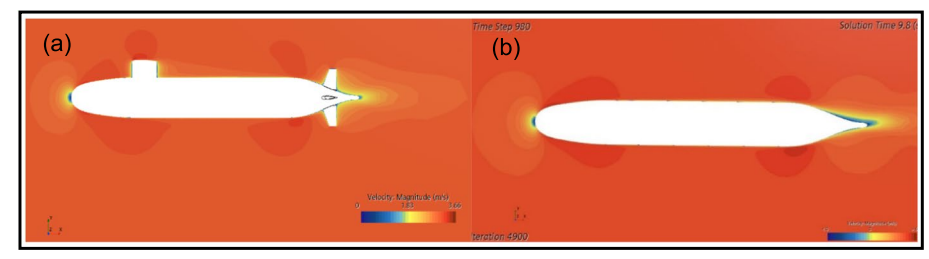


Fig. 11 Velocity depiction of DARPA SUBOFF: a fully appended hull form, b bare hull form

some areas around the sail, stern, and hull that are higher. More refinement is needed in these areas to further improve accuracy. Nevertheless, this boundary grid is used for simulations reported here because the values at the majority of points are within the required *y*+ range, and the accuracy in drag reported earlier is within 2% at zero pitch.

# Longitudinal control in hydrodynamics with varying angle of stern appendages

In this part the dynamic simulation of DARPA SUBOFF is applied to calculate hydrodynamic variables at a velocity of 3.05 m/s. DARPA SUBOFF analyses were carried out with rigid body movement from  $-20^{\circ}$  to  $+20^{\circ}$  AoAs. This data of CFD was then compared with the experimental static data at different AoAs from literature. The simulation has been executed with deflection of control surfaces (stern appendages) at multiple angles of attack from  $-30^{\circ}$  to  $+30^{\circ}$ .

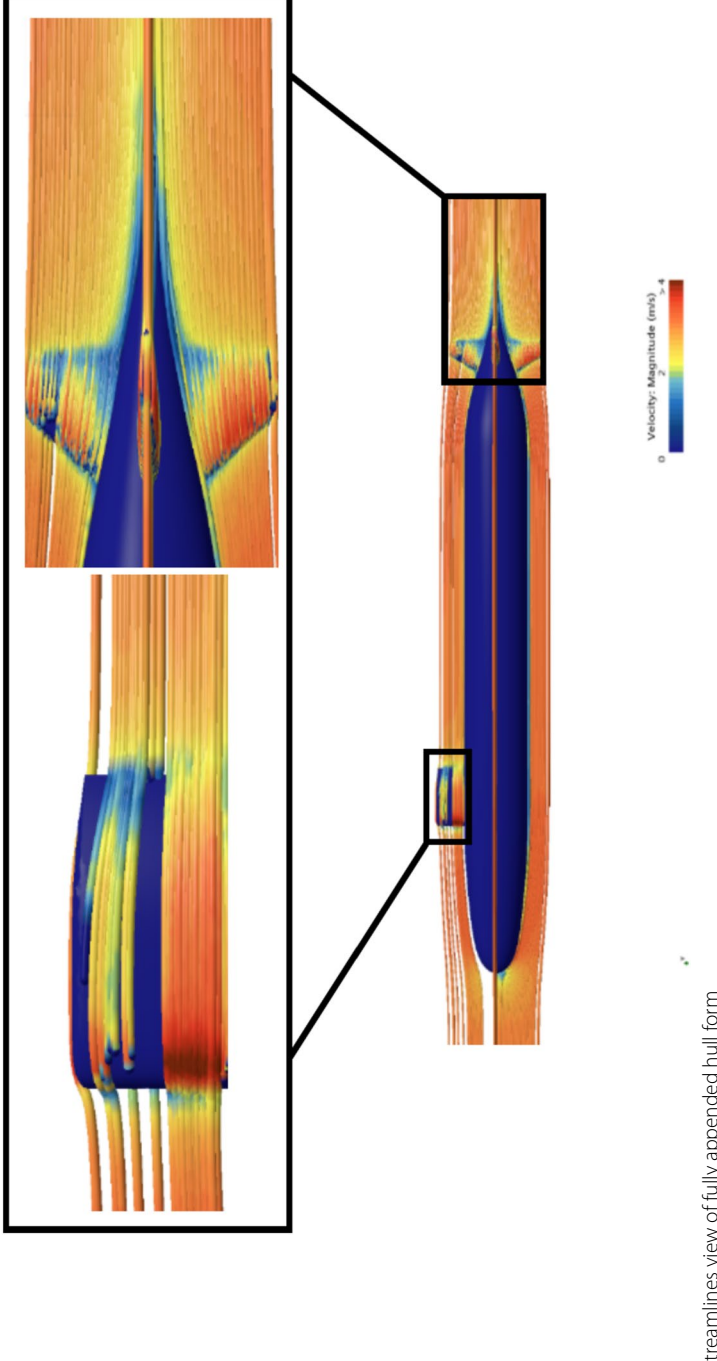
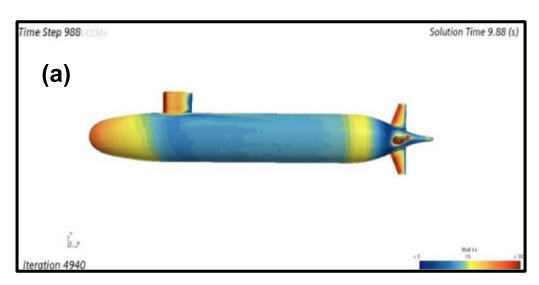


Fig. 12 Streamlines view of fully appended hull form



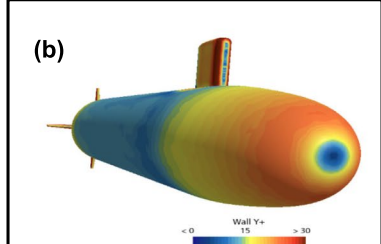
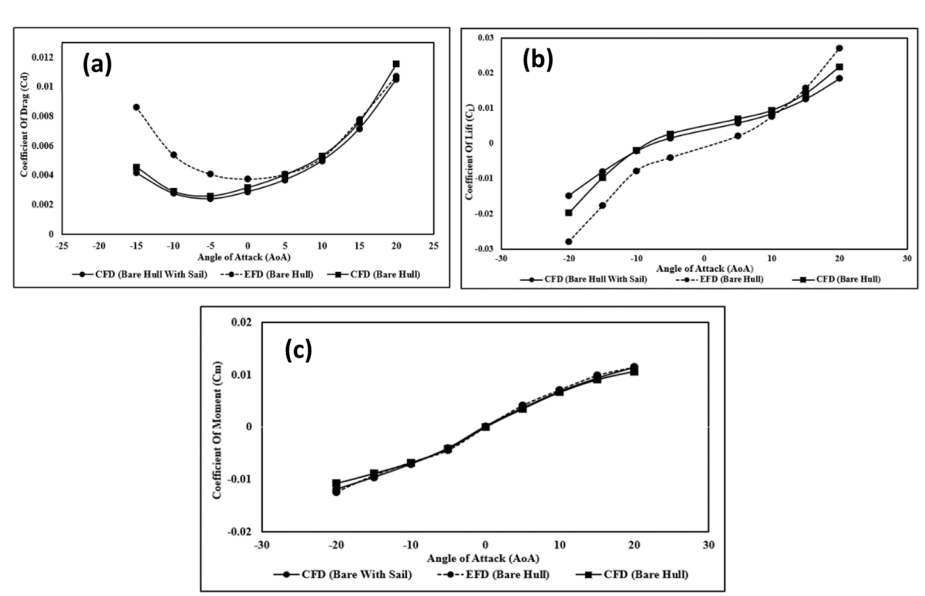


Fig. 13 Wall y+ depiction at 3.05 m/s: a side view, b front view

At V=3.05 m/s, a confirmation investigation of dynamic simulation of DARPA SUB-OFF was carried out of bare hull and bare hull with sail from  $-20^{\circ}$  to  $+20^{\circ}$  AoA ( $\alpha$ ). Drag force, lift force, moment, and their coefficients were calculated from the CFD simulations. Equations (6), (7), and (8) were then used to calculate the coefficients of drag, lift, and moment, correspondingly. Tonio, A.S et al. presented the experimental findings of bare hull form in their article [32]. The findings of the experiments and the outcomes of the CFD were then contrasted. The results of the validation study are presented in Fig. 14.

It may be noted that when CFD is compared to the experimental outcomes at the highest positive AoA, drag coefficient estimation of bare hull results shows a variance of around 7%, while the drag coefficient prediction of bare hull with sail shows an error of about -2% shown above in Fig. 14a. This suggests that when it comes to drag estimations, bare hull with sail shows near results as compared to bare hull without sail.

Figure 14b also compares the  $C_{\rm L}$  at 3.05 m/s produced using Star CCM+ with the outcomes of the experimental data. When CFD is compared to the experimental outcomes at the highest positive AoA,  $C_{\rm L}$  prediction of bare hull without sail results shows a variance of around - 19%, while the  $C_{\rm L}$  prediction of bare hull with sail shows an error of about - 31%. Therefore, it is generally the most suitable fit for researching flow dynamics.



**Fig. 14** Comparison of hydrodynamic coefficients at 3.05 m/s with experimental results: **a** drag coefficient. **b** Lift coefficient. **c** Pitching moment coefficient

Similarly, the moment force coefficient obtained using Star CCM+ with the outcomes of the experimental data is depicted in Fig. 14c. When CFD is compared to the experimental outcomes at the highest positive AoA, moment force coefficient estimation of bare hull without sail results shows a variance of around -7%, while the moment force coefficient prediction of bare hull with sail shows an error of about -0.14%. The largest inaccuracy produced at the highest AoA in the scenario of the moment values is -7%. In addition to this, the forces and moments trends are in contrast with their respective coefficients.

# Hydrodynamic variables obtained at varying pitch angles and stern appendage angles

The drag, Lift, and moment forces and their coefficients result at multiple AoAs at 3.05 m/s speed with deflection of control surfaces from  $-30^{\circ}$  to  $+30^{\circ}$  dynamically are shown in Figs. 12, 13, 14, 15, 16, and 17. Figure 15a, b shows the correlation of drag force and its coefficient with deflection of the control surfaces ( $-30^{\circ}$  to  $+30^{\circ}$ ) at various AoAs. It is depicted from the figure that as the submersible vehicle rotates from  $-30^{\circ}$  to  $+30^{\circ}$  dynamically, the value of drag force and its coefficient increases dramatically. At small angles of control surfaces, the numerical value of drag force and its coefficient is lower and near other values of control surfaces as compared to larger angles of control surfaces. At negative AoA, the value of drag force and its coefficient is lower, and at positive AoA, the value of drag force and its coefficient is higher. Figures 16a, b depicts the relationship between lift forces and their coefficient, respectively, with the static deflection of the control surfaces ( $\pm 30^{\circ}$ ) at a velocity of 3.05 m/s at different AoAs. The image shows how the lift force and its coefficient substantially rise as the submersible vehicle turns dynamically from -30 to  $+30^{\circ}$ . The magnitude

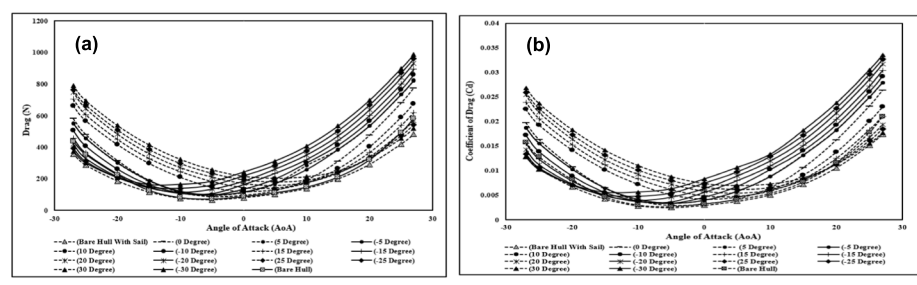


**Fig. 15** Comparison of hydrodynamic parameters at 3.05 m/s with deflection of control surfaces: **a** drag force. **b** Drag coefficient

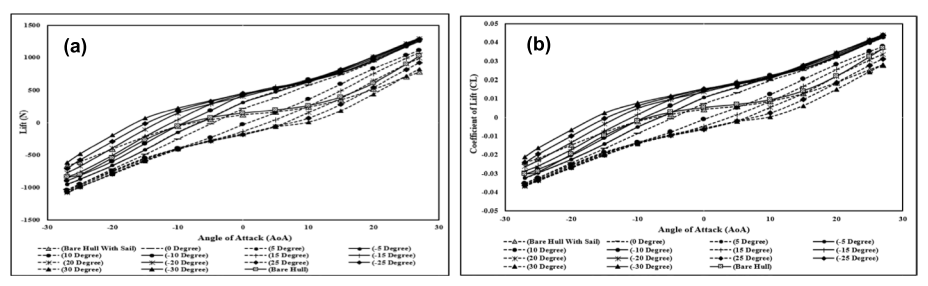


**Fig. 16** Comparison of hydrodynamic parameters at 3.05 m/s with deflection of control surfaces: **a** lift force. **b** Lift coefficient

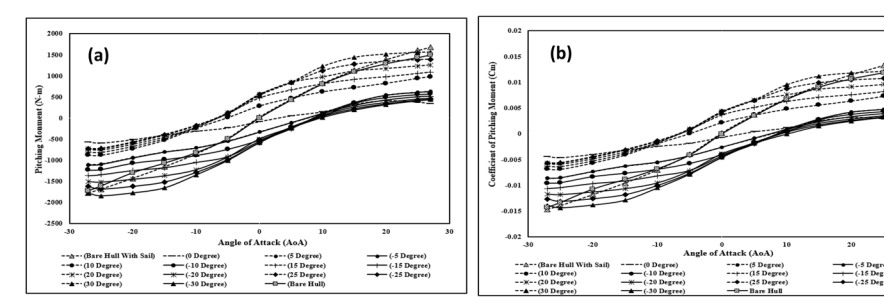


**Fig. 17** Comparison of hydrodynamic parameters at 3.05 m/s with deflection of control surfaces: **a** pitching moment. **b** Pitching moment coefficient

of the lift force and its coefficient are both negative at negative AoAs, while they are both positive at positive AoA. When the AoA is above  $\pm$  10°, the lift for all the control surfaces angles coalesce to close to the same values, as can be seen in Fig. 15. This indicates that the control surface has stalled and cannot generate further increases in moment. Figures 17a, b shows an excellent connection between moment forces and their coefficient, correspondingly. The figure further demonstrates the effect of submersible vehicle dynamic rotation from - 30° to + 30° causing the moment force and its coefficient to significantly increase. At negative AoAs, the value of moment and coefficients are both negative, but at positive angles, they are both positive.

The plots of drag, lift, and moment forces as well as coefficients with deflection of the control surfaces ( $-30^{\circ}$  to  $+30^{\circ}$ ) at velocities of 5.14 m/s and 6.10 m/s at different AoAs were also calculated. Outcomes display a similar pattern in all hydrodynamic variables as in the scenario of a velocity of 3.05 m/s, although the values will rise significantly as the velocity rises. In comparison to greater angles of control surfaces (stern appendages), the values of drag forces, lift forces, and moments are numerically smaller and closer to other values of control surfaces for small angles of control surfaces. It may be noted that when the AoA is negative, the hydrodynamic variables and their coefficients have a lower value, and when the AoA is positive, they have a higher value. It may also be noted that as the velocity of UVs increases, the numerical values of hydrodynamic parameters rise accordingly, but their coefficients remain the same.

Moreover, it is found that as the speed is increased the Cd varies from 5 to 6% at various speeds demonstrating the increase in the drag of the body. However, Cm and  $C_L$  demonstrated an ascending trend for the increase in parameters with the change in the angle AoA of the body.

One notifiable parametric change in the Cm trends shows a systematic change either way from control surface increment and decrement. This trend can further be flourished using a 3rd Order ordinary differential equation, i.e., provided from Eqs. (9)-(11);

$$Cm = -3\alpha^{3} \times E^{-07} - 7\alpha^{2} \times E^{-07} + 0.0005\alpha - 0.0051$$
(9)

$$Cm = -2\alpha^{3} \times E^{-07} - 1\alpha^{2} \times E^{-06} + 0.0007\alpha + 6 \times E^{-05}$$
(10)

$$Cm = -3\alpha^{3} \times E^{-07} - 1\alpha^{2} \times E^{-06} + 0.0005\alpha + 0.0041$$
(11)

Where variable y represents the  $C_{\rm m}$  varying due to the change in AoA which is an independent term, i.e., x here. By using Eqs. (9)–(11) one can predict the Cm of the DARPA. By looking at the Eq. from (9) to (11), it is quantified that the change in Cm Line for a 0° control surface angle when presented with the applying 3rd order polynomial intercept equation depicted above by Eq. (10) demonstrates an ascending increment. In addition to this, when the last variable of each Eqs. (9) to (11) (i.e., coefficients with  $x^0$ ) are considered, we observe that constants are increasing; however, the coefficients attributed to the power terms are almost similar. This shows that the constant value with  $x^0$  demonstrates tangible variation with the change in the AoA. These equations can be of great help to construct the mathematical algorithm for control augmentation systems. This data array with transient simulation demonstrates that by having detailed analysis for a complete set of AoAs can provide comprehensive insight in formulating equations for hydrodynamic performance predictions.

### Flow field using 20° stern appendage at varying AoA

The velocity contours of the body rotated dynamically from  $-30^{\circ}$  to  $+30^{\circ}$  with a deflection of control surfaces (stern appendages) at a  $+20^{\circ}$  deflection angle are depicted in Fig. 18. Wall y+ value of the body rotated dynamically from  $-30^{\circ}$  to  $+30^{\circ}$  with a deflection of control surfaces (stern appendages) at five different deflection angles was also calculated. However, the  $10^{\circ}$  deflection of the control surface at  $30^{\circ}$  AoA is depicted in Fig. 19.

The streamlines contour of the body rotated dynamically from  $-30^{\circ}$  to  $+30^{\circ}$  with deflection of control surfaces (i.e., stern appendages) at five different deflection angles was also calculated. However, -10° deflection of control surface at 30° AoA is depicted

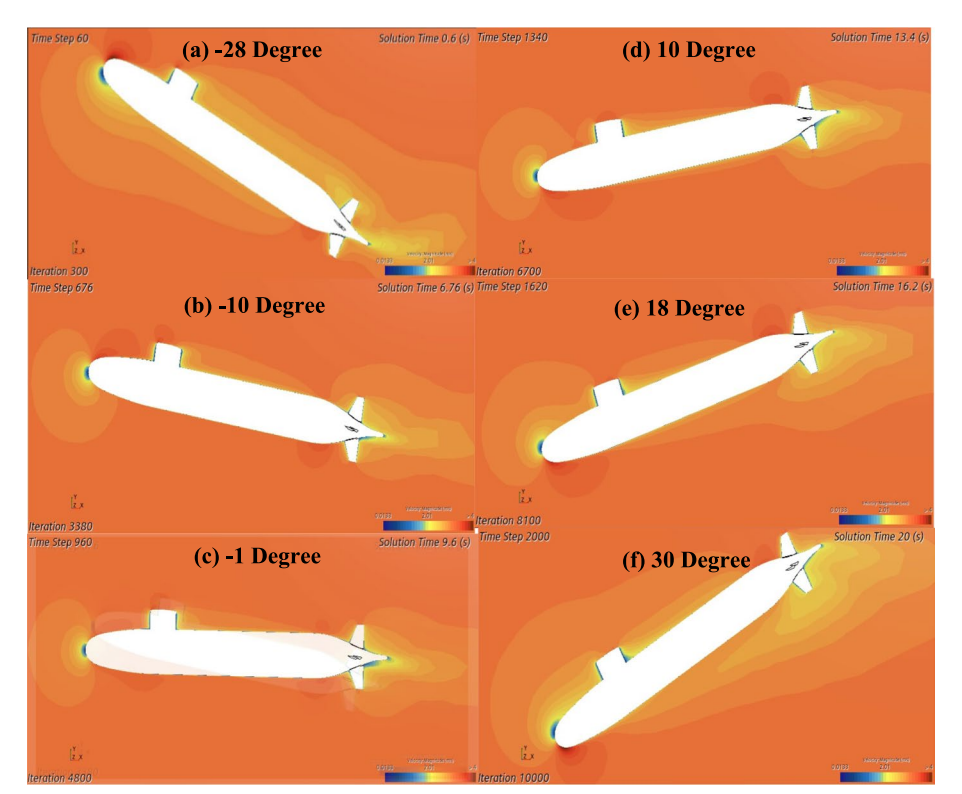


**Fig. 18** Velocity depiction with different angle of attacks with  $+20^{\circ}$  control surfaces (stern appendages) actuation:  $\mathbf{a}-28^{\circ}$ ,  $\mathbf{b}-10^{\circ}$ ,  $\mathbf{c}-1^{\circ}$ ,  $\mathbf{d}10^{\circ}$ ,  $\mathbf{e}18^{\circ}$ ,  $\mathbf{f}30^{\circ}$ 

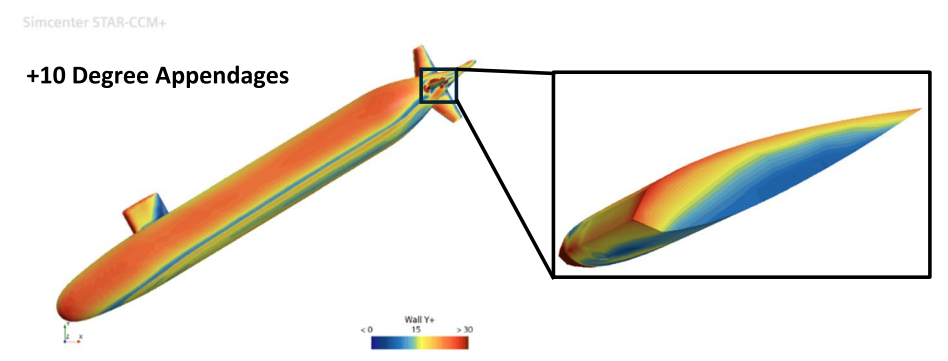
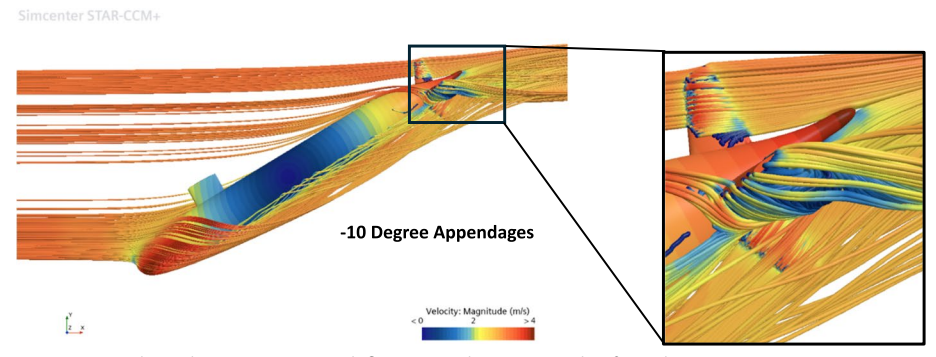


Fig. 19 Wall y+ depiction at 10° deflection angles at 30° angle of attack

in Fig. 20. A representation of the fluid flow across the DARPA SUBOFF is shown in the form of streamlines in Fig. 20. Star CCM+ was used to generate illustrative visualizations. Although Star CCM+ only allowed a limited number of streamlines to be selected to reduce calculating time. The vortices generated at the stern appendages are due to large pressure gradients. Furthermore, findings that are highly comparable have been derived from Star CCM+. At smaller AoAs, flows are generally identical in pattern, but as the AoA changes from  $-30^{\circ}$  to  $+30^{\circ}$ , the variation of flow as well as the hydrodynamic parameters on CFD changes. This might be because of the turbulence model that is the use of the Navier-Stokes Equations and other differential equations in CFD. Additionally, CFD calculates the boundary layer attachment and detachment over the body's surface. Shear stresses close to the surface of the body can also be examined by comprehensive CFD study.

The vector depiction of DARPA SUBOFF rotated dynamically from  $-30^{\circ}$  to  $+30^{\circ}$  with deflection of control surfaces (i.e., stern appendages) at  $+20^{\circ}$  deflection angle was also analyzed.

From Fig. 20, it is depicted that due to higher changes in AoA, horseshoe vortex creates underneath the appendages. This horseshoe vortex can cause the erosion of surface, thereby protruding towards less efficacious control surface operation. However, the amount of circulation of flow underneath the appendage demonstrates high pressure as the intensity of velocity there is low, which will provide tangible boundary layer attachment below the control surface for causing pitching moment of the complete body.



**Fig. 20** Streamlines depiction at  $-10^{\circ}$  deflection angles at 30° angle of attack

### **Conclusions**

The present study offers a variety of data points that are preferable for developing control algorithms and offer more authority on the control surface or AoA controllability/ maneuverability. The study presented here should be carefully considered before being put into practice. To the best of our knowledge, the most recent submersible incident was attributed to its reliance on thruster-based propulsion instead of the intended control surfaces. At extreme depths, the increasing hydrostatic pressure may have compromised thruster performance, as their operational limits could have been exceeded. This scenario aligns with known challenges in deep-sea environments, where pressureinduced mechanical failures are a critical concer. It can be inferred that if it had a control surface along with thrusters or a hybrid system, it might have been able to overcome the pressure at that depth. Moreover, the addition of a control surface would have allowed thrusters to work efficiently within their optimal range, avoiding exacerbating power consumption and instability. It would have added a safety factor to level two as per design criteria. The current study has also demonstrated that causing small deflections using control surfaces can help in altering the pressure over the body, causing an immediate change in the orientation of the underwater vehicle. However, thrusters require a lot of energy from batteries for optimum operation, which is not the case for control surfaces.

Dynamic models are crucial for simulating complex underwater motions prior to the launching of the UVs. A key component of this dynamic simulation of UVs is the estimation of the force and moment coefficients. The upper Limit of dimensionless hydrodynamic parameters from the dynamic pitch maneuver of the DARPA SUBOFF for i.e., drag, Lift, and pitching moment coefficients at 3.05 m/s speed were approximately found to be 0.035, 0.05, and 0.015 respectively. The other speeds were accordingly calculated. Moreover, hydrodynamic variables at various AoAs, with deflection of control surfaces ranging from - 30° to + 30° for stern appendages were analyzed and trends were found to be with minimum error.

### **Abbreviations**

UVs Under water vehicles

DARPA Defense Advanced Research Projects Agency

Cd Coefficient of drag

AoA Angle of attack

Cm Coefficient of pitching moment

C<sub>L</sub> Coefficient of lift

CFD Computational fluid dynamics
PIV Particle image velocimetry

RANS/LES Revnolds Average Navier Stokes / Large Eddies Simulation

URANS Unsteady Reynolds-Averaged Navier-Stokes
DDES Delayed Detached Eddy Simulations
FW-H Ffowcs Williams and Hawkings equation

### Acknowledgements

Not applicable.

### Authors' contributions

IM: first author, manuscript writing, execution, and simulation work. AL: second author, manuscript writing, editing, supervision of the work. AN: third author, editing and reviewing. GR: fourth author, formatting and reviewing. JK: fifth author, English check. AH: sixth author, formatting, and reviewing.

### Funding

There is no funding associated with this research.

### Data availability

Data will be made available on request.

### **Declarations**

### **Competing interests**

The authors declare that they have no competing interests.

Received: 24 February 2025 Accepted: 13 August 2025

Published online: 12 September 2025

### References

- Abkowitz MA (1969) Stability and motion control of ocean vehicles. MIT, The MIT Press, Printed in the USA, Card Nr, Massachusetts Institute of Technology, pp 70–93041
- Alin N, Fureby C, Svennberg S, Sandberg W, Ramamurti R, Wikstrom N, Bensow R, Persson T (2005). 3D unsteady
  computations for submarine-like bodies. In 43rd AlAA Aerospace sciences meeting and exhibit, pp. 1104.
- Aqilah F, Islam M, Juretic F, Guerrero J, Wood D, Ani FN (2018) Study of mesh quality improvement for CFD analysis of an airfoil. IIUM Engineering Journal 19(2):203–212
- Hussain A, Loya A, Riaz Z, Malik SA (2023) To study the effectiveness of stern appendages (Cruciform & X Shaped configurations) for maneuverability of autonomous underwater vessel using computational fluid dynamics. Ocean Engineering 272:113858. https://doi.org/10.1016/j.oceaneng.2023.113858
- Cao L-S, Zhu J, Wan W-B (2016) Numerical investigation of submarine hydrodynamics and flow field in steady turn. China ocean engineering 30(1):57–68
- Caplier C, Rousseaux G, Calluaud D, David L (2020) Effects of finite water depth and lateral confinement on ships wakes and resistance. J Hydrodynamics 32:582–590
- Cardenas P, de Barros EA (2019) Estimation of AUV hydrodynamic coefficients using analytical and system identification approaches. IEEE J Oceanic Eng 45(4):1157–1176
- 8. Carrica P, Kim Y, Martin J (2021) Vertical zigzag maneuver of a generic submarine. Ocean Eng 219:108386
- 9. Cho YJ, Seok W, Cheon K-H, Rhee SH (2020) Maneuvering simulation of an X-plane submarine using computational fluid dynamics. Int J Nav Arch Ocean Eng 12:843–855
- 10. Deville MO (2022) An introduction to the mechanics of incompressible fluids, Springer Nature, pp. 325.
- Dreyer JJ, Boger DA (2010) Validation of a free-swimming, guided multibody URANS simulation tool. In 28th Symposium on Naval Hydrodynamics. Pasadena California.
- 12. Gong Y, Xie J, Xu J, Chen Z, He Y, Cai S (2022) Oceanic internal solitary waves at the Indonesian submarine wreckage site. Acta Oceanologica Sinica 41(3):109–113. https://doi.org/10.1007/s13131-021-1893-0
- Groves NC, Huang TT, Chang MS (1989) Geometric characteristics of DARPA (Defense Advanced Research Projects Agency) SUBOFF models (DTRC model numbers 5470 and 5471) (No. DTRCSHD129801).
- Hao Y, Ding J, Bian C, Zhao P, Xia L, Wang X, Liu H (2024) Deep graph learning for the fast prediction of the wake field of DARPA SUBOFF. Ocean Eng 309:118353. https://doi.org/10.1016/j.oceaneng.2024.118353
- He X, Wang L, Huang Q, Li H, Liu J (2025) Numerical analysis of the effect of a breaking-vortex baffle around appendage on the submarine flow field and flow noise. Ocean Eng 319:120284. https://doi.org/10.1016/j.oceaneng.2024. 120284
- 16. Heberley BD (2011) Analysis of the operational impacts of alternative propulsion configurations on submarine maneuverability (Doctoral dissertation, Massachusetts Institute of Technology).
- 17. Hui L, Jinyun P, Tao J (2009) Research on submarine maneuverability of flooded compartment. In 2009 International Conference on Computer Technology and Development (Vol. 2, pp. 149-152). IEEE.
- 18. Kim H, Hong SK (2011) Numerical study on the hydrodynamic control derivatives of a high-speed underwater vehicle with X-stern configuration. J Mech Sci Technol 25:3075–3082
- Kim J, Kim K, Choi HS, Seong W, Lee K-Y (2002) Estimation of hydrodynamic coefficients for an AUV using nonlinear observers. IEEE J Oceanic Eng 27(4):830–840
- 20. Leong ZQ, Ranmuthugala D, Penesis I, Nguyen HD (2015) RANS-based CFD prediction of the hydrodynamic coefficients of DARPA SUBOFF geometry in straight-line and rotating arm manoeuvres. International Journal of Maritime Engineering, 157(A1), pp. 41–51.
- 21. Li P, Deng H, Xu B, Xia W, Yi W (2025) Modeling the hydrodynamic pressure field and wake field characteristics of an underwater vehicle and studying their correlation. J Mar Sci Eng 13(1):85
- 22. Lihong W, Xisheng F, Zuolin Y, Yiping L (2021) Physics-based simulation of AUV forced diving by self-propulsion. J Shanghai Jiaotong Univ 55(3):290
- Lin Y-H, Lee M-C, Hasan AD (2024) The hydrodynamic analysis of the fully appended DARPA SUBOFF model in the SPMM tests integrating the LES model with the dynamic mesh method. J Mech 40:732–758. https://doi.org/10. 1093/jom/ufae057
- 24. Lin Y-H, Lu P-Y, Lin C-W (2019) Numerical simulation of maximum wave loads and run-up heights on offshore wind turbine foundations influenced by the instability of bichromatic wave groups. Mar Struct 67:102648
- 25. Liu HL, Huang TT (1998) Summary of DARPA SUBOFF experimental program data (No. CRDKNSWCHD129811).
- Mitra A, Panda JP, Warrior HV (2024) The hydrodynamic characteristics of autonomous underwater vehicles in rotating flow fields. Proceedings of the Institution of Mechanical Engineers, Part M: Journal of Engineering for the Maritime Environment, 238(3), 691-703.

- 27. Pankajakshan R (2002) Validation of control-surface induced submarine maneuvering simulations using UNCLE. In Proceedings of 24th symposium on naval hydrodynamics, Fukuoka, Japan, 8-13 July 2002.
- 28. Posa A, Balaras E (2020) A numerical investigation about the effects of Reynolds number on the flow around an appended axisymmetric body of revolution. J Fluid Mech 884:A41
- Roddy RF (1990) Investigation of the stability and control characteristics of several configurations of the DARPA SUBOFF model (DTRC Model 5470) from captive-model experiments (No. DTRCSHD129808).
- 30. Shahinfar E, Bozorg M, Bidoky M (2010) Parameter estimation of an AUV using the maximum likelihood method and a Kalman filter with fading memory. IFAC Proc Vol 43(16):1–6
- 31. Shin H-W, Paik K-J, Jang Y-H, Eom M-J, Lee S (2020) A numerical investigation on the nominal wake of KVLCC2 model ship in regular head waves. Int J Nav Arch Ocean Eng 12:270–282
- 32. Tonio AS, Krishna HR, Issac MT (2022) Estimation of force and moment coefficients for DARPA SUBOFF using USAF DATCOM method. In OCEANS 2022-Chennai (pp. 1-6). IEEE.
- 33. Toxopeus S, Atsavapranee P, Wolf E, Daum S, Pattenden R, Widjaja R, Gerber A (2012) Collaborative CFD exercise for a submarine in a steady turn. In International Conference on Offshore Mechanics and Arctic Engineering (Vol. 44922, pp. 761-772). American Society of Mechanical Engineers.
- 34. Wang S, Sun J, Zhao B, Yun Y, Huang B (2022) Numerical study on the interaction between ocean current power generator and unmanned underwater vehicle. J Mar Sci Eng 10(12):1869
- 35. White FM, Majdalani J (2006) Viscous fluid flow (Vol. 3, pp. 433-434). New York: McGraw-Hill.
- 36. Whitfield CC (1999) Steady and unsteady force and moment data on a DARPA2 submarine (Doctoral dissertation, Virginia Tech).
- 37. Zhang H, Xu Y-R, Cai H-P (2010) Using CFD software to calculate hydrodynamic coefficients. J Mar Sci Appl 9:149–155

### **Publisher's Note**

Springer Nature remains neutral with regard to jurisdictional claims in published maps and institutional affiliations.